Biosensors and Bioelectronics 94 (2017) 507–512

Contents lists available at ScienceDirect

Biosensors and Bioelectronics

journal homepage: www.elsevier.com/locate/bios

# Pd-Au@carbon dots nanocomposite: Facile synthesis and application as an ultrasensitive electrochemical biosensor for determination of *colitoxin* DNA in human serum

Qitong Huang[a,b], Xiaofeng Lin[a], Jie-Ji Zhu[a], Qing-Xiao Tong[a,*]

[a] Department of Chemistry, Shantou University, Shantou 515063, PR China
[b] Department of Food and Biological Engineering, Zhangzhou Institute of Technology, Zhangzhou 363000, PR China

ARTICLE INFO

*Keywords:*
DNA biosensor
Carbon dots
Banana peels
Pd-Au@Carbon dots nanocomposite

ABSTRACT

In this study, a green and fast method was developed to synthesize high-yield carbon dots (CDs) via one-pot microwave treatment of banana peels without using any other surface passivation agents. Then the as-prepared CDs was used as the reducing agent and stabilizer to synthesize a Pd-Au@CDs nanocomposite by a simple sequential reduction strategy. Finally, Pd-Au@CDs nanocomposite modified glassy carbon electrode (Pd-Au@CDs/GCE) was obtained as a biosensor for target DNA after being immobilized a single-stranded probe DNA by a carboxyl ammonia condensation reaction. Under the optimal conditions, the sensor could detect target DNA concentrations in the range from $5.0\times10^{-16}$ to $1.0\times10^{-10}$ mol $L^{-1}$. The detection limit (LD) was estimated to be $1.82\times10^{-17}$ mol $L^{-1}$, which showed higher sensitivity than other electrochemical biosensors reported. In addition, the DNA sensor was also successfully applied to detect *colitoxin* DNA in human serum.

## 1. Introduction

During the last few years, the interest to detect target DNA has been dramatically increased due to great significance of their application in biosensors, clinical-diagnosis, pharmaceutical-analysis and et al. (Heerema and Dekker, 2016; Kugelberg, 2015; Evtugyn and Hianik, 2016; Guo et al., 2017; Huang et al., 2015a). Therefore, many classic methods have been developed for determination of DNA, such as quartzcrystal microbalance (Rasheed and Sandhyarani, 2016; Furusawa et al., 2016), electrochemiluminescence (Yang et al., 2016a), fluorescence (Dziuba et al., 2016; Liu and Su, 2017), surface plasmon resonance spectroscopy (Ghrera et al., 2016; Halpern et al., 2013), electrochemistry (Xu et al., 2015a; Yuan et al., 2016; Diculescu et al., 2016; Zheng et al., 2014a; Chen et al., 2015) and so on. Compared with other techniques, the electrochemistry offers broad opportunities in DNA biosensor, owning to their advantages of high sensitivity, simplicity, low-cost and portability. For example, Zheng et al. (2014a) used CdS/poly-isonicotinic acid/glassy carbon electrode (GCE) for determination of *colitoxin* DNA (detection limit (LD) $=3.90\times10^{-15}$). Chen et al. (2015) employed the rugby-ball-shaped $CoS_2$-Poly(2-thiophenesulfonyl chloride)/GCE to detect *colitoxin* DNA (LD=$1.10\times10^{-14}$). For determination of DNA, most of electrochemical techniques have made many important contributions. However, their systems have either low sensitivity or the modified materials was complex, expensive and ungreen. Therefore, it is urgent to develop a DNA biosensor which not only has high sensitivity, high selectivity and good reliability, but also is simple, economical and green.

In the past decades, nanomaterials have been widely used in biosensors due to their excellent chemical, physical and biological properties (Liu et al., 2014a, 2014b; Cheng et al., 2014; Xue et al., 2015; Han et al., 2015; Hou et al., 2015). Carbon dots (CDs), as a new star carbon material, has been used for fabricating electrochemical sensors due to their low cytotoxicity, excellent biocompatibility, ultra-high electrocatalysis properties and large surface area (Du and Guo, 2016; Huang et al., 2015b; Zhang et al., 2015a; Han et al., 2016; Li et al., 2016). Meanwhile, CDs also can be used as reductant and stabilizer, which can reduce the $Au^+$, $Ag^+$, $Cu^{2+}$ or graphene oxide to Au nanoparticle (Dao et al., 2016), Ag nanoparticle (Choi et al., 2013), $Cu_2O$ nanoparticle (Huang et al., 2015c) and reduced graphene oxide (Hong et al., 2016), respectively. Many attempts have recently been made to prepare CDs from natural sources, which are widely available and harmless to the environment. However, most of these CDs have a relatively low yield, which limits their practical applications (Gu et al., 2016). Therefore, it remains imperative to search for a low-cost precursor even litter serving as a carbon source to develop a green,

* Corresponding author.
*E-mail address:* qxtong@stu.edu.cn (Q.-X. Tong).

http://dx.doi.org/10.1016/j.bios.2017.03.048
Received 17 December 2016; Received in revised form 2 March 2017; Accepted 21 March 2017
Available online 22 March 2017
0956-5663/ 

simple and rapid synthesis of CDs with high-yield on large scale.

As known, recent reports show that nanoalloys can construct the miniaturization of functional units and develop the novel electrochemical systems because of their excellent electrochemical behavior. For biosensing electrodes, Pd-Au nanoalloy is a good candidate in electrochemical biosensors due to its large surface area, good biocompatibility, remarkable conductivity and so on (Zhou et al., 2016; Xu et al., 2015; Wang et al., 2015; Sharma et al., 2016; Zheng et al., 2016). For example, Xu et al. (2015b) synthesized porous Au@Pd core-shell nanostructure for the determination of thrombin. Wang et al. (2015) reported $TiO_2$-Au/Pd nanoparticles for the determination of cluster of differentiation 146 antigen. Sharma et al. (2016) used Au-Pd/boron-nitride nanosheets as the catalytic labels for array protein.

In this work, a green and economic method was developed for preparation of CDs with high-yield. The litter banana peels was used as a carbon source for microwave synthesis of hydrosoluble high-conductivity CDs without using any surface passivation agents. Then a new nanocomposite containing Pd-Au@carbon dots (Pd-Au@CDs) was obtained by using CDs as the stabilizing and mild reducing agent. The nanocomposite was further casted on glassy carbon electrode (GCE) surface before DNA immobilization. Electrochemical experiments indicated the probe DNA could be feasibly anchored on the Pd-Au@CDs/GCE surface via coupling with the carboxyl group of CDs. Meanwhile, this biosensor exhibited high electric conductivity due to the existence of Pd-Au@CDs. Hybridization experiments showed a wide range from $5.0\times10^{-16}$ to $1.0\times10^{-1}$° mol $L^{-1}$ for the target DNA concentrations with the LD of $1.82\times10^{-17}$ mol $L^{-1}$ by using the methylene blue (MB) as indicator. At the same time, the complementary, non-complementary or base-mismatched sequences could be well distinguished by the biosensor. In addition, this biosensor was applied successfully to determine DNA in human serum.

## 2. Experimental

### 2.1. Reagents and apparatus

Methylene blue (MB), 1-(3-Dimethylaminopropyl)-3-ethylcarbodiimide hydrochloride (EDC), EDTA, Tris (hydroxymethyl) aminomethane (Tris) and N-Hydroxy succinimide (NHS) were obtained from Sinopharm Chemical Reagent Co., Ltd.

24-base oligonucleotide sequence for *colitoxin* were chosen in this study (Shenggong Bioengineering Co., Ltd.) (Zheng et al., 2014a, Chen et al., 2015):

Probe DNA (S1): 5′-$NH_2$-$(CH_2)$6-GAG CGG CGC AAC ATT TCA GGT CGA-3′;

Complementary sequence (S2): 5′- TCG ACC TGA AAT GTT GCG CCG CTC-3′;

One-base-mismatch sequence (S3): 5′-TCG ACC TGA AAT GTT GCG CC***T*** CTC-3′;

Three-base mismatched sequence (S4): 5′-TCG ***T***CC TGA AA***C*** GTT GCG CC***T*** CTC-3′;

Non-Complementary sequence (S5): 5′-GCA CGG CGC AAC ATT TCA GGT CGA-3′.

Electrochemical experiments were performed on a CHI 660D electrochemical analyzer. Three-electrode system: a bare or modified GCE as working electrode, a Pt wire as auxiliary electrode and an Ag/AgCl as reference electrode. UV–vis absorption experiments were recorded by mapada UV-1800PC. Transmission electron microscope (TEM) and energy dispersive X-ray spectrometer (EDAX) was measured on a JEM-1230 electron microscope. X-ray diffraction (XRD) patterns were carried out on a GBC MMA X-ray diffractometer. X-ray photoelectron spectroscopy (XPS) measurements were obtained on a PHI 5000 VersaProbe. Fourier transform infrared spectroscopy (FT-IR) was carried out on a Spectrum GX FTIR system (PerkinElmer). Raman spectra were recorded on a Micro Raman system from Jobin Yvon Horiba LABRAM-HR visible with a 633 nm He-Ne laser beam.

### 2.2. Synthesis of CDs

4.0g fresh banana peels were added into 50 mL water and stirred for 10 min. Then the mixture was transferred to a domestic 500 W microwave oven and heated for 20 min. After cooling, the obtained solution was centrifuged at 5000 rpm for 30 min to remove large particles. Then the obtained solution was filtered through a 0.45 mm membrane and dialyzed for 36 h with the dialysis membranes of 1200 cutoffs. Finally, the solution was lyophilized for obtaining dry CDs. After the calculation, the yield of CDs was about 16.0%, which is higher than some reports (Gu et al., 2016).

### 2.3. Synthesis of Pd-Au@CDs

Synthesis of Pd-Au@CDs was similar to that of synthesis of Au@CDs (Dao et al., 2016). First, 100 μL aqueous solution of $HAuCl_4$ (0.5 mg $mL^{-1}$) and 100 μL aqueous solution of $H_2PdCl_4$ (0.5 mg $mL^{-1}$) was added to 100 μL CDs solution (8.0 mg $mL^{-1}$). Then the mixed solution was put into a water bath and keep at 90 °C for 60 min to obtain the purple solution of Pd-Au@CDs.

### 2.4. Synthesis of the Pd-Au@CDs/GCE

The bare GCE electrode was polished with 0.5 μm, 0.3 μm and 0.05 μm α-alumina, respectively, then rinsed with $H_2O$, absolute ethanol and $H_2O$, in turn (Huang et al., 2016). After that, 10 μL Pd-Au@CDs composite solution was modified on the GCE, and dried at 35 °C to form Pd-Au@CDs/GCE. For comparison, other work electrodes were also prepared in the same way.

### 2.5. Covalent immobilization of S1 on the Pd-Au@CDs/GCE and the hybridization reaction

DNA immobilization was performed by using EDC/NHS as linking reagents (Shen et al., 2016). Pd-Au@CDs/GCE was first immersed into 1 mL 50.0 μmol $L^{-1}$ PBS containing 5.00 mmol $L^{-1}$ EDC and 5.00 mmol $L^{-1}$ NHS for 20 min to preactivate the carboxylic groups of CDs. Then using TE (10 mmol $L^{-1}$ Tri-HCl, 1.0 mmol $L^{-1}$ EDTA, pH=8.0) to rinse, 10 μL 0.1 μmol $L^{-1}$ S1 was pipetted onto Pd-Au@CDs/GCE. After drying, the covalent reaction was finishing. The S1/Pd-Au@CDs/GCE was put into 200 μL different targets (in TE buffer solution) for 35 min at 35 °C. Finally, it was rinsed with TE buffer solution to dislodge the un-hybridized targets. The scheme of this electrochemical DNA biosensor was shown in Fig. 1.

## 3. Results and discussion

### 3.1. Characterization of materials

Fig. 2**A** showed the typical UV–visible absorption spectra of CDs, Au@CDs, Pd@CDs and Pd-Au@CDs. The CDs had an absorption peak at 281 nm, which might be attributed to the π-π* transition of CDs (Chen et al., 2013). Au@CDs had two strong absorption peaks at 282 nm and 538 nm. The absorption peak at 538 nm was the surface plasmon resonance (SPR) absorption of the AuNPs (Metin et al., 2013). These results indicated that CDs could reduce $AuCl_4^-$ to Au@CDs, while the Pd@CDs did not have SPR absorption peak, as shown in Fig. 2**A**, which could explain that the increase of electron density in Au nanoparticle upon forming alloy with Pd (Zhang et al., 2015b). The Pd-Au@CDs nanoparticles were further characterized by X-ray diffraction (XRD) measurements in Fig. 2**B**. The XRD peak at 18.3 °corresponded to the (002) crystal plane of CDs (Chen et al., 2013). At the same time, they had intense XRD peaks at 37.4°, 45.1°, 64.3° and 78.5°, which corresponded to the Pd-Au nanoparticles' crystal planes: (111), (200), (220) and (311) (Huang et al., 2016). The results were consistent with previous reports. X-ray photoelectron spectrometer

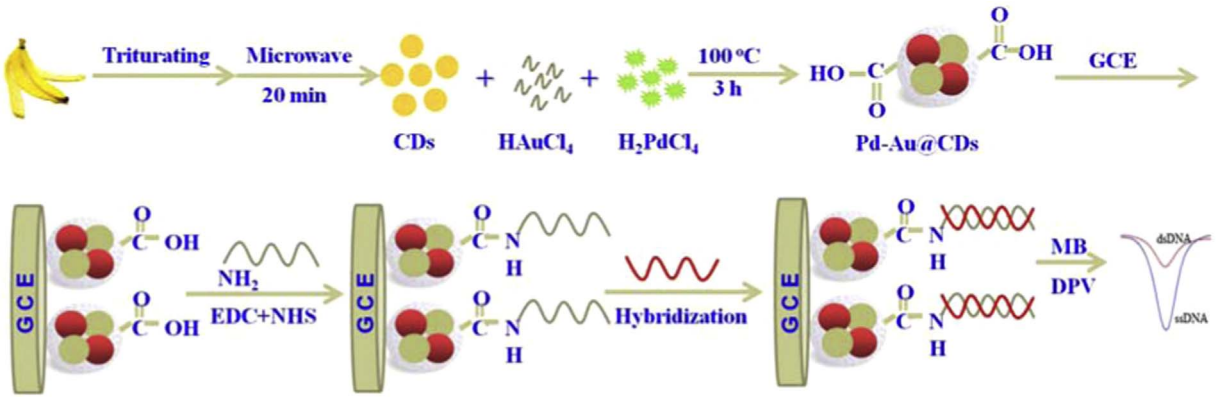


**Fig. 1.** Microwave assisted one-step green synthesis of high-yield CDs from banana peels: application as the reductant and stabilizer for synthesizing Pd-Au@CDs to detect colitoxin DNA.

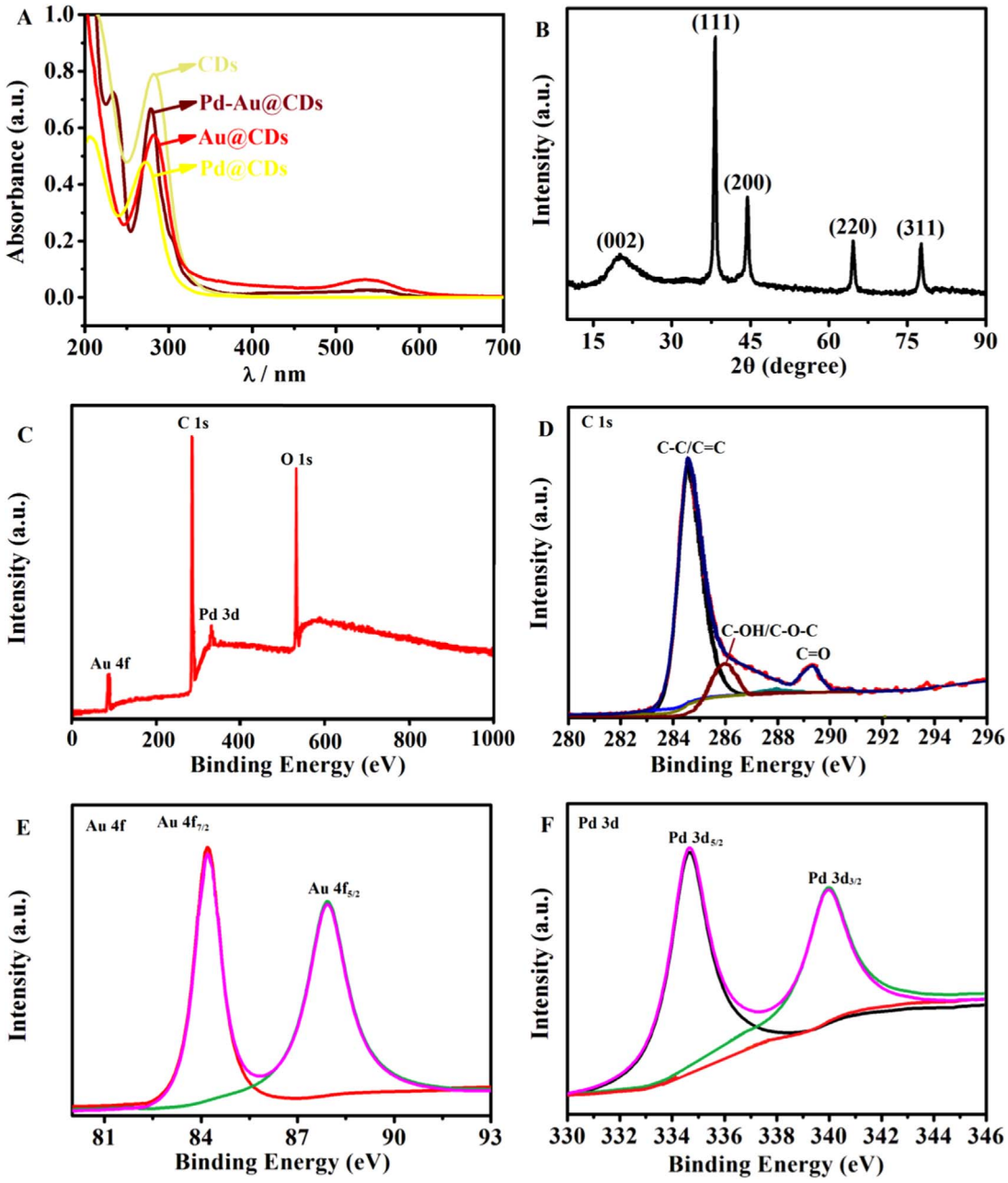


**Fig. 2.** (A) UV–vis spectra for CDs, Au@CDs, Pd@CDs and Pd-Au@CDs, (B) XRD pattern for the obtained Pd-Au@CDs, (C) XPS survey spectrum of Pd-Au@CDs, high resolution XPS spectra of (D) C 1s, (E) Au 4f and (F) Pd 3d in the Pd-Au@CDs.

(XPS) measurements were also performed to make further characterization of Pd-Au@CDs nanoparticles (Fig. 1C). The peaks of C 1s, Au 4f and Pd 3d of the Pd-Au@CDs were shown in Fig. 2**(D)**, **(E) and (F)**, respectively. The C 1s peaks appeared at 284.7 eV, 286.6 eV and 288.2 eV, which was attributed to the C–C/C=C, C–OH/C-O-C and C=O bonds, respectively. Au 4f peaks appeared at 84.06 eV and 87.88 eV, indicating the formation of metallic $Au^0$ in the nanocomposite. Meanwhile, the peaks of Pd 3d at 334.8 eV and 340.3, which were the typical peaks of $Pd^0$, suggested that the $PdCl_4^{2-}$ could be reduced to $Pd^0$ by CDs (Huang et al., 2016; Li et al., 2015). TEM showed the average diameter of the CDs (Fig. S1**A**) was determined to be 2.2 ± 0.8 nm. As shown in Fig. S1**B and** Fig. S1**C**, the average diameter of the Au@CDs and Pd@CDs were determined to be 6 ± 1.0 nm and 16 ± 1.0 nm, respectively. Fig. S1**D** showed that the sizes of Pd-Au@CDs ranged from 5 to 15 nm. From the HRTEM image (Fig. S1**E**), the lattice spacing was 0.205 nm, which corresponded to the (002) planes' lattice spacing of CDs, and the (111) planes' lattice spacing of Au/Pd corresponded to the lattice spacing was 0.317 nm. Fig. S1**F** showed the selected area electron diffraction (SAED) pattern of Pd-Au@CDs displayed high crystallinity and the ring patterns corresponding to the Pd-Au nanometal with polycrystalline structures were observed (Zheng et al., 2014b; Lv et al., 2014). Moreover, the EDAX (Fig. S2) also revealed the formation of Au-Pd@CDs nanocrystals in this work.

Raman spectra of CDs and Au@CDs were shown in Fig. S3. The spectrum of CDs does not show any Raman signal under our measurement conditions because of its strong fluorescence background (Zhu et al., 2013; Luo et al., 2012). However, the Raman spectrums of Au@CDs, Pd@CDs and Pd-Au@CDs exhibited typical bands of carbon nanocrystals at ca. 1356 $cm^{-1}$ (D band) and 1586 $cm^{-1}$ (G band). These spectral observations also implied that the strong fluorescence of CDs in Au@CDs, Pd@CDs and Pd-Au@CDs were partly quenched via the photoinduced electron transfer from CD shells to Au, Pd or Pd-Au cores, indicating that CDs were firmly coated on Au, Pd and Pd-Au nanoparticles (Luo et al., 2012). Fig. S4 showed the typical IR spectra of CDs, Au@CDs, Pd@CDs and Pd-Au@CDs. The characteristic peak of hydroxyl groups (-OH) at 3438 $cm^{-1}$ and carbonyl groups (C=C) at 1650 $cm^{-1}$ were observed in the spectrum of CDs (De and Karak, 2013). Comparing with CDs, the relative intensity of hydroxyl groups (-OH) decreased and the intensity of carbonyl groups (C=O, 1725 $cm^{-1}$) increased after reaction with $HAuCl_4$, indicating that hydroxyl groups (-OH) on the surface of CDs might play an important role in reducing of $HAuCl_4$ into Au@CDs (Yang et al., 2016b). At the same time, the main characteristic peak in the spectra of Pd@CDs and Pd-Au@CDs were similar to that of Au@CDs. All above results indicated that Pd-Au@CDs was prepared successfully.

### 3.2. Cyclic voltammetric and electrochemical impedance spectroscopy behavior of electrodes

The different electrodes were characterized by CVs. From Fig. 3**A**, on bare GCE, there was a pair of reversible redox peaks corresponding to $[Fe(CN)_6]^{3-/4-}$. The reduction ($I_{pc}$) and oxidation ($I_{pa}$) peak currents were at 3.24 μA and −6.63 μA, respectively. While the GCE was coated with CDs, the $I_{pc}$ and $I_{pa}$ were increased to 4.67 μA and −8.31 μA, respectively, suggesting that the CDs' film could accelerate the electron transfer kinetic of $[Fe(CN)_6]^{3-/4-}$, which might be due to the excellent electrocatalysis of CDs. When GCE was coated with Au@CDs, the $I_{pc}$ and $I_{pa}$ were increased to 10.59 μA and −13.18 μA, respectively. Also, after casting the Pd@CDs on GCE, the $I_{pc}$ and $I_{pa}$ were increased to 7.5 μA and −10.4 μA, respectively. However, the Pd-Au@CDs/GCE had the strongest signals ($I_{pc}$=16.22 μA and $I_{pa}$=−23.12 μA), which indicated that the application of Pd-Au@CDs could dramatically promote the sensitivity of the electrochemical biosensor.

The different electrodes were also characterized by electrochemical impedance spectroscopy (EIS). As shown in Fig. 3**B**, the electrode-transfer resistance (Ret) value was 242 Ω on the GCE. While on CDs/GCE the Ret value was 198 Ω, which also could attribute to the presence of high conductive CDs accelerating the electron transfer kinetic of $[Fe(CN)_6]^{3-/4-}$. On Pd@CDs/GCE, Au@CDs/GCE and Pd-Au@CDs/GCE, the Ret values were 147 Ω, 99 Ω and 23 Ω, respectively. The results showed that the Pd-Au@CDs/GCE had the best electrochemical performance. Hence, this was also strongly proved that Pd-Au@CDs/GCE could be a promising platform for electrochemical DNA biosensor.

### 3.3. CV characterization on DNA immobilization

CVs of 1.0 mmol $L^{-1}$ $[Fe(CN)_6]^{3-/4-}$ at Pd-Au@CDs/GCE before and after immobilization with S1 were shown in Fig. S5. After reaction with S1, the redox peak currents ($I_p$) of $[Fe(CN)_6]^{3-/4-}$ showed increase as compared with case of without immobilization with S1, suggesting that S1/Pd-Au@CDs/GCE had better electrochemical performance in $[Fe(CN)_6]^{3-/4-}$. The reason was the negative carboxyl groups on Pd-Au@CDs were covalently bound with the amino groups on S1, which reduced the negative-charge density of electrode surface. It suggested that S1 could be successfully immobilized to the surface of Pd-Au@CDs/GCE via a condensation reaction.

### 3.4. Hybridization detection using MB as indicator

As the electrochemical indicator, methylene blue (MB) has been widely applied for DNA hybridization due to its interaction with guanine (Hu et al., 2012). In this study, MB was used to monitor the hybridization of the DNA biosensor. The interaction time of MB with

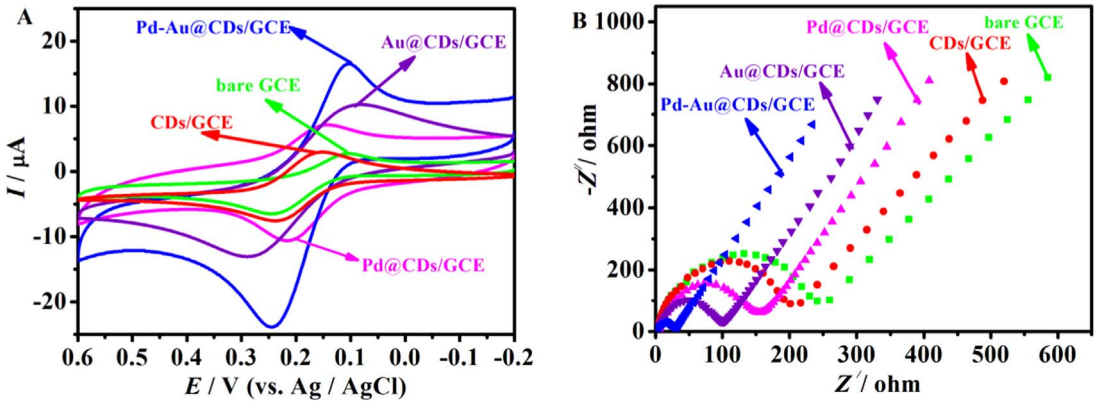


**Fig. 3.** Cyclic voltammograms (A) and EIS (B) of GCE, CDs/GCE, Pd@CDs/GCE, Au@CDs/GCE, Pd-Au@CDs/GCE in 1.0 mmol $L^{-1}$ $[Fe(CN)_6]^{3-/4-}$ solution containing 0.1 mol $L^{-1}$ KCl (The scan rate of 100 mV $s^{-1}$ and the scan direction was from −0.2 to 0.6 V).

the probe DNA was investigated. Fig. S6 showed that as time-intervals for accumulation of MB was prolonged, the signals of MB were intensified, and then leveled off to a saturation value after 30 min of accumulation. In this study, 35 min was chosen as the optimal reaction time to achieve the highest sensitivity of the DNA biosensor.

Through the scan rate ($\upsilon$), we studied the control factors of electrochemical process on the S1/Pd-Au@CDs/GCE. As shown in Fig. S7, the $I_p$ increase linearly with the scan rate, suggesting that the process was surface-controlled process. Fig. S7**B** showed the linear relationship between $I_p$ and scan rates. The $I_{pa}$ and $I_{pc}$ showed good linear relationship with $\upsilon$, and the linear equations were $I_{pa}$ (μA) $=-136.427\ \upsilon$ (V $s^{-1}$) $-0.127$ ($r^2$=0.9988) and $I_{pc}$ (μA)$=120.804\ \upsilon$ (V $s^{-1}$) $+0.579$ ($r^2$=0.9996), respectively.

The surface density of S1 on the electrode could influence the sensitivity of DNA hybridization assay. It could be calculated by the MB's electrochemical signal. In our experiments, the quantity of electric charge for MB was $4.33\times10^{-5}$ C. The quantity of MB on the S1/Pd-Au@CDs/GCE surface was $2.25\times10^{-10}$ mol according to the following equation:

$$N = Q/neN_A$$

Where $N$ was the amount of MB; $Q$ was the electric-charge amount of MB; $n$=2, which was the electrons' number; $e=1.6\times10^{-19}$ C, which was one electron's charge quantity; $N_A=6.02\times10^{23}$ $mol^{-1}$, which was Avogadro's number. The surface coverage of S1 was calculated from the quantity of MB, 1 mol MB reacted with 1 mol guanine in S1. The surface density of S1 on the Pd-Au@CDs/GCE surface (diameter 2 mm) was $5.73\times10^{-10}$ mol $cm^{-2}$.

### 3.5. Analytical performance of the sensors

Differential pulse voltammetry (DPV) for the signals of MB at S1 immobilized Pd-Au@CDs/GCE and after hybridization with S2, S3, S4 and S5 were shown in Fig. 4. On the S1/Pd-Au@CDs/GCE, the signal of MB was strongest, because of the reaction between MB and the free guanine bases. After hybridizing with S2, the MB's signal was toboggan, due to the fact that the interaction of MB and guanine residues of the probe was prevented by duplex formation on S1/Pd-Au@CDs/GCE. After S1/Pd-Au@CDs/GCE hybridizing with S3, the signal of MB was different. The difference indicated the hybridization was not complete reaction. When S1/Pd-Au@CDs/GCE hybridized with S5, the $I_{pa}$ did not decline nearly, suggesting that hybridization was not reaction. These results indicated that only S2 could form a complete double-strand DNA on the S1/Pd-Au@CDs/GCE, also indicated the high selectivity of this biosensor.

For determining the LD of this biosensor, target DNA was analyzed

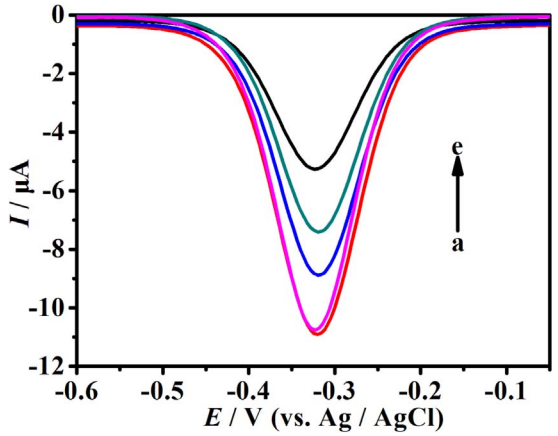


**Fig. 4.** DPV responses of $1.00\times10^{-5}$ mol $L^{-1}$ of MB for the Pd-Au@CDs/GCE without hybridization (a), after hybridized with $5.00\times10^{-11}$ mol $L^{-1}$ S5 (b), S4 (c), S3 (d) and S2 (e).

in the presence of different concentration. Fig. 5**A** was obtained that the MB signal decreased with increasing concentration of target DNA ranged from 0 to $1.00\times10^{-10}$ mol $L^{-1}$. The hydrogen bonding interaction of MB with dsDNA was considered to play a significant role for the increased $I_{pa}$ responses of dsDNA than that of ssDNA. As seen in Fig. 5**B**, there was a liner relationship between $I_{pa}$ and target DNA's concentration ranged from $5.00\times10^{-16}$ to $1.00\times10^{-10}$ mol $L^{-1}$. The regression equation was $I_{pa}/(1.0\times10^{-6}\ A)=-2.189\ \lg(C_{S2}/mol\ L^{-1})\ -5.590$ (n=6, $R^2$=0.9985). The low LD was $1.82\times10^{-17}$ mol $L^{-1}$, which showed this biosensor had higher sensitivity than other electrochemical biosensors reported (Table 1).

### 3.6. Reproductivity, regeneration and stability of the biosensor

In this study, the reproductivity of this DNA biosensor was measured by six parallel experiments for DNA biosensors to detect $1.0\times10^{-15}$ mol $L^{-1}$ target DNA, and the relative standard deviation (RSD) was 2.03% (n=6), indicating the reproductibility of this DNA biosensor was good. Putting S1/Pd-Au@CDs/GCE at 4 $^0$C for two weeks, from the DPV responses, the result was in a change of 1.2%, showing that this DNA biosensor had a good stability. The experiment of regeneration was done as following: putting the S1/Pd-Au@CDs/GCE into 1.00 mol $L^{-1}$ NaOH for 8 min, then hybridizing with S2 in buffer solution. By this way, the DNA biosensor was almost regeneration.

### 3.7. Detection of target DNA in human serum

In order to evaluate the applicability of this biosensor in real sample, the target DNA was detected in human serum. The human serum with or without the addition of the target DNA wasstudied with the biosensor. The DPV signals in Fig. S8 were decreased a little in human serum because of the interference of the sample matrix during the hybridization between target DNA and S1, Which indicated the sensor had high selectivity in real sample. From Fig. S8, it could be seen that a lower concentration of target DNA ($2.0\times10^{-11}$ mol/L) was still could be detected in human serum. These results suggested this biosensor was a promising analytical platform for detecting target DNA in human serum.

## 4. Conclusion

In this paper, a green method was developed to synthesize high-yield carbon dots (CDs). And Pd-Au@CDs nanocomposite was easily obtained by using the as-prepared CDs as the reducing agent and stabilizer through a simple sequential reduction strategy. The Pd-Au@CDs nanocomposite modified GCE and immobilized with S1, and the S1/Pd-Au@CDs was as a platform for detection of target sequence related to *colitoxin* gene with good stability, ultrahigh sensitivity and excellent specificity. The DNA biosensor was also applied to determine *colitoxin* DNA in human serum.

## Acknowledgement

This research was supported by the National Natural Science Foundation of China (Project 51673113 and 51273108), the National Basic Research Program of China (973 Program no. 2013CB834803), the Education Bureau of Fujian Province (Project no. JAT160875) the Natural Science Foundation of Zhangzhou (Project no. ZZ2016J31) and the Training Program Foundation for Excellent Youth Researching Talents of Fujian's Universities (Fujian Education Section, No. 2016-23). This work was also supported by open fund of Fujian Provincial Key Laboratory of Modern Analytical Science and Separation Technology (Minnan Normal University).

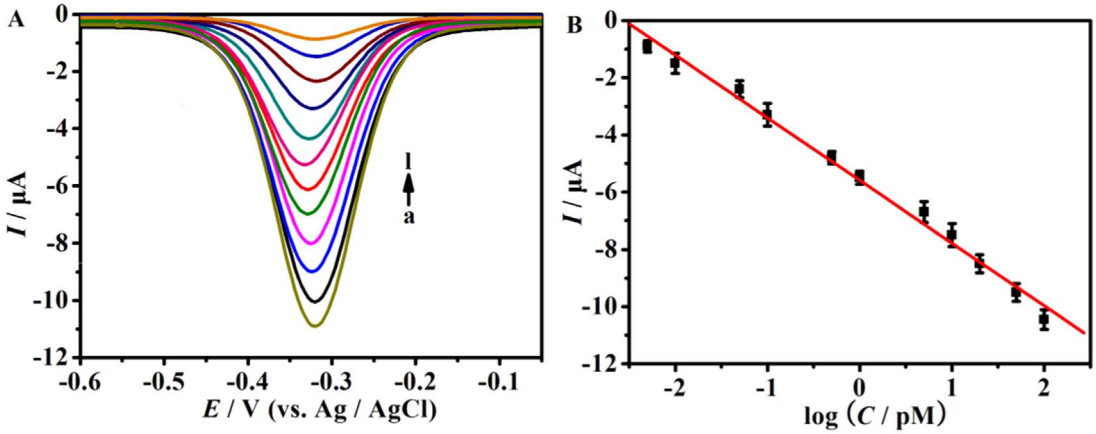


**Fig. 5.** (A) DPVs responses of $1.00\times10^{-5}$ mol $L^{-1}$ of MB for different DNA hybrids. Concentration of target DNA: a to k: 0, 0.00500, 0.0100, 0.0500, 0.100, 0.500, 1.00, 5.00, 10.0, 20.0, 50.0, 100.0 pM. (B) Linear relationship between the DPV peak current change and the logarithm of the target DNA concentration.

**Table 1**
Comparison of the different electrochemical biosensors for colitoxin DNA.

| Electrode | Detection technique | Linear range (M) | Detection limit (M) | Reference |
|---|---|---|---|---|
| Rutin-Mn/MWCNTs/GCE | DPV | $1.60\times10^{-9}$ to $4.80\times10^{-8}$ | $3.81\times10^{-11}$ | Niu et al. (2008) |
| 1-aminopyrene/grapheme/GCE | EIS | $1.00\times10^{-12}$ to $1.00\times10^{-8}$ | $4.50\times10^{-13}$ | Luo et al. (2013) |
| CdS/poly-isonicotinic acid/GCE | DPV | $1.00\times10^{-14}$ to $1.00\times10^{-9}$ | $3.90\times10^{-15}$ | Zheng et al. (2014a) |
| Morin-Co (II) /MWCNTs/GCE | DPV | $2.00\times10^{-9}$ to $5.00\times10^{-10}$ | $8.10\times10^{-11}$ | Niu et al. (2014) |
| Rugby-Ball-Shaped $CoS_2$ -Poly(2-thiophenesulfonyl chloride)/GCE | DPV | $1.00\times10^{-13}$ to $1.00\times10^{-7}$ | $1.10\times10^{-14}$ | Chen et al. (2015) |
| Pd-Au@CDs/GCE | DPV | $5.00\times10^{-16}$ to $1.00\times10^{-10}$ | $1.82\times10^{-17}$ | This work |

## Appendix A. Supplementary material

Supplementary data associated with this article can be found in the online version at http://dx.doi.org/10.1016/j.bios.2017.03.048.

## References


Chen, B., Li, F., Li, S., Weng, W., Guo, H., Guo, T., Zhang, X., Chen, Y., Huang, T., Hong, X., You, S., Lin, Y., Zeng, K., Chen, S., 2013. Nanoscale 5 (5), 1967–1971.
Chen, X., Wang, Q., Wang, L., Guo, H., Yang, Y., Li, F., Gao, F., 2015. Ind. Eng. Chem. Res. 54 (5), 1520–1528.
Cheng, J., Han, Y., Deng, L., Guo, S., 2014. Anal. Chem. 86 (23), 11782–11788.
Choi, H., Ko, S.J., Choi, Y., Joo, P., Kim, T., Lee, B.R., Jung, J.W., Choi, H.J., Cha, M., Jeong, J.R., Hwang, I.W., Song, M.H., Kim, B.S., Hwang, I.W., 2013. Nat. Photonics 7 (9), 732–738.
Dao, V.D., Kim, P., Baek, S., Larina, L.L., Yong, K., Ryoo, R., Ko, S.H., Choi, H.S., 2016. Carbon 96, 139–144.
De, B., Karak, N., 2013. RSC Adv. 3, 8286–8290.
Diculescu, V.C., Chiorcea-Paquim, A.M., Oliveira-Brett, A.M., 2016. TrAC Trend Anal. Chem. 79, 23–36.
Dziuba, D., Jurkiewicz, P., Cebecauer, M., Hof, M., Hocek, M., 2016. Angew. Chem. 128 (1), 182–186.
Du, Y., Guo, S., 2016. Nanoscale 8, 2532–2543.
Evtugyn, G., Hianik, T., 2016. TrAC-Trend Anal. Chem. 79, 168–178.
Furusawa, H., Nakayama, H., Funasaki, M., Okahata, Y., 2016. Anal. Biochem. 492, 34–42.
Ghrera, A.S., Pandey, M.K., Malhotra, B.D., 2016. Biosens. Bioelectron. 80, 477–482.
Gu, D., Shang, S., Yu, Q., Shen, J., 2016. Appl. Surf. Sci. 390, 38–42.
Guo, Y., Chen, Q., Qi, Y., Xie, Y., Qian, H., Yao, W., Pei, R., 2017. Biosens. Bioelectron. 87, 320–324.
Halpern, A.R., Wood, J.B., Wang, Y., Corn, R.M., 2013. ACS Nano 8 (1), 1022–1030.
Han, Y., Chabu, J.M., Hu, S., Deng, L., Liu, Y.N., Guo, S., 2015. Chem. Eur. J. 21 (37), 13045–13051.
Han, C., Wang, R., Wang, K., Xu, H., Sui, M., Li, J., Xu, K., 2016. Biosens. Bioelectron. 83, 229–236.
Heerema, S.J., Dekker, C., 2016. Nat. Nanotechnol. 11 (2), 127–136.
Hong, T.Z., Xue, Q., Yang, Z.Y., Dong, Y.P., 2016. J. Power Sources 303, 109–117.
Hou, L., Wu, X., Chen, G., Yang, H., Lu, M., Tang, D., 2015. Biosens. Bioelectron. 68, 487–493.
Hu, Y., Wang, K., Zhang, Q., Li, F., Wu, T., Niu, L., 2012. Biomaterials 33 (4), 1097–1106.
Huang, H., Bai, W., Dong, C., Guo, R., Liu, Z., 2015a. Biosens. Bioelectron. 68, 442–446.
Huang, Q., Lin, X., Li, F., Weng, W., Lin, L., Hu, S., 2015a. Prog. Chem. 27 (11), 1604–1614.
Huang, Q., Lin, X., Lin, C., Zhang, Y., Hu, S., Wei, C., 2015b. RSC Adv. 5 (67), 54102–54108.
Huang, Q., Lin, X., Lin, C., Zhang, Y., Zhang, H., Hu, S., Wei, C., Tong, Q.X., 2016. Anal. Methods 8 (33), 6347–6352.
Kugelberg, E., 2015. Nat. Rev. Immunol. 15 (4), 200–201.
Li, Q., Huang, Q., Zhu, J.J., Ji, W.G., Tong, Q.X., 2016. RSC Adv. 6 (90), 87230–87236.
Li, S.S., Hu, Y.Y., Wang, A.J., Weng, X., Chen, J.R., Feng, J.J., 2015. Sens. Actuators B: Chem. 208, 468–474.
Liu, J., Morris, M.D., Macazo, F.C., Schoukroun-Barnes, L.R., White, R.J., 2014a. J. Electrochem. Soc. 161, H301–H313.
Liu, J., Wagan, S., Morris, Dávila, Taylor, M., White, J., R. J, 2014b. Anal. Chem. 86, 11417–11424.
Liu, Z., Su, X., 2017. Biosens. Bioelectron. 87, 66–72.
Luo, P., Li, C., Shi, G., 2012. Phys. Chem. Chem. Phys. 14 (20), 7360–7366.
Luo, L.Q., Zhang, Z., Ding, Y.P., Deng, D.M., Zhu, X.L., Wang, Z.X., 2013. Nanoscale 5 (13), 5833–5840.
Lv, J.J., Li, S.S., Wang, A.J., Mei, L.P., Chen, J.R., Feng, J.J., 2014. Electrochim. Acta 136, 521–528.
Metin, Ö., Sun, X., Sun, S., 2013. Nanoscale 5 (3), 910–912.
Niu, S.Y., Cui, H.H., Shen, X.T., Wu, M.L., 2014. Asian J. Chem. 26 (9), 2578–2582.
Niu, S., Zhao, M., Hu, L., Zhang, S., 2008. Sens. Actuators B: Chem. 135 (1), 200–205.
Rasheed, P.A., Sandhyarani, N., 2016. Anal. Chim. Acta 905, 134–139.
Sharma, M.K., Narayanan, J., Pardasani, D., Srivastava, D.N., Upadhyay, S., Goel, A.K., 2016. Biosens. Bioelectron. 80, 442–449.
Shen, Q., Fan, M., Yang, Y., Zhang, H., 2016. Anal. Chim. Acta 934, 66–71.
Wang, Y., Li, Y., Ma, H., Guo, A., Du, B., Yan, T., Wei, Q., 2015. Analyst 140 (10), 3557–3564.
Xu, B., Zheng, D., Qiu, W., Gao, F., Jiang, S., Wang, Q., 2015a. Biosens. Bioelectron. 72, 175–181.
Xu, W., Yi, H., Yuan, Y., Jing, P., Chai, Y., Yuan, R., Wilson, G.S., 2015b. Biosens. Bioelectron. 64, 423–428.
Xue, Q., Liu, Z., Guo, Y., Guo, S., 2015. Biosens. Bioelectron. 68, 429–436.
Yang, L., Tao, Y., Yue, G., Li, R., Qiu, B., Guo, L., Z. Yang, Lin, H. H, 2016a. Anal. Chem. 88 (10), 5097–5103.
Yang, L., Liu, X., Lu, Q., Huang, N., Liu, M., Zhang, Y., Yao, S., 2016b. Anal. Chim. Acta 930, 23–30.
Yuan, R., Ding, S., Yan, Y., Zhang, Y., Zhang, Y., Cheng, W., 2016. Biosens. Bioelectron. 77, 19–25.
Zhang, L., Han, Y., Zhu, J., Zhai, Y., Dong, S., 2015a. Anal. Chem. 87 (4), 2033–2036.
Zhang, Z., Cao, S.W., Liao, Y., Xue, C., 2015b. Appl. Catal. B: Environ. 162, 204–209.
Zheng, D., Wang, Q., Gao, F., Wang, Q., Qiu, W., Gao, F., 2014a. Biosens. Bioelectron. 60, 167–174.
Zheng, J.N., Li, S.S., Ma, X., Chen, F.Y., Wang, A.J., Chen, J.R., Feng, J.J., 2014b. J. Power Sources 262, 270–278.
Zheng, Y., Yuan, Y., Chai, Y., Yuan, R., 2016. Biosens. Bioelectron. 79, 86–91.
Zhou, Q., Lin, Y., Lin, Y., Wei, Q., Chen, G., Tang, D., 2016. Biosens. Bioelectron. 78, 236–243.
Zhu, S., Meng, Q., Wang, L., Zhang, J., Song, Y., Jin, H., Zhang, Kai., Sun, H., Wang, H., Yang, B., 2013. Angew. Chem. Int. Edit. 52 (14), 3953–3957.